A reconfigurable LNA with compact magnetic-capacitive coupling transformer networks for 5G 28-/39-GHz applications

Depeng Cheng, Xin Chen, Qin Chen, Xujun Ma, Lianming Li

A Reconfigurable LNA with Compact Magnetic-Capacitive Coupling Transformer Networks for 5G 28/39 GHz Applications

Depeng Cheng, *Member, IEEE*, Xin Chen, Graduate *Student Member, IEEE*, Qin Chen, Xujun Ma, *Member, IEEE*, Lianming Li, *Member, IEEE*

***Abstract*—This letter presents a frequency reconfigurable low noise amplifier (LNA) for 5G 28/39 GHz bands applications. In the proposed LNA, a wideband input common-source amplifier is designed to cover both 28 and 39 GHz bands, and following two parallel switchable common-gate amplifiers are leveraged to split the RF signal into two independent signal paths. Thus, the output single-band amplifiers could be optimized flexibly at each target operating band with area-efficient magnetic-capacitive coupling transformer-based matching networks, improving the amplifier power gain, noise figure, and out-of-band signal rejection performance. Fabricated in a 65-nm CMOS process, the proposed LNA has a compact die size of only 0.1 mm^2, and achieves 16.6/15 dB peak gain, 4.06/4.46 dB minimum NF, and -12.1/-16.5 dBm IP1dB at 28/39 GHz bands, respectively, while consuming 26.4 mW from a 1.2-V power supply.**

***Index Terms*—Low noise amplifier, reconfigurable, CMOS, 28/39 GHz bands, magnetic-capacitive coupling transformer.**

I. Introduction

With the advancement of the fifth-generation (5G) new radio (NR) standards, fully integrated mm-wave phase array transceivers to support 28/39 GHz 5G FR2 bands are getting attractive [1-4]. To this end, considering the co-existing 28/39 GHz bands, it is very critical to implement dual-band low-noise amplifier (LNA) with competitive overall performance, especially the out-of-band signal rejection, while considering chip area overhead.

Various techniques have been proposed to realize multi-band LNAs for 5G mm-wave noncontiguous bands. Based on the realization topologies, they could be categorized as concurrent wideband, and band-switching solutions. In previous works, wideband LNAs are typically realized with multi-resonance impedance matching network [5], negative feedback [6], and multi-pole tuning techniques [7-9], but they usually suffer from poor out-of-band signal rejection performance. On top of that, concurrent LNAs further use notch filters with high quality factor to suppress out-of-band interferences, thereby achieving high communication capacity and reliability [10,11]. Nevertheless, to achieve concurrent wideband designs, all the active gain cells and passive elements need to serve for strict in-band gain flatness, and the circuit performance in each target operating band is compromised. In contrast, the band-switching LNAs utilize tunable passive elements to configure the circuit for each target operating band [12-14]. However, limited by the passive elements loss, such solution lacks the optimization flexibility to improve the circuit performance.

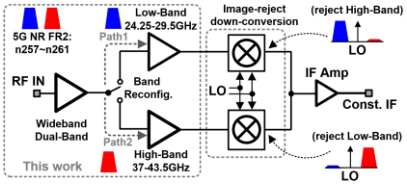

Fig. 1. Block diagram of the proposed 5G 28/39GHz receiver including the frequency reconfigurable LNA.

To address above issues, Fig. 1 shows the proposed block diagram of the 5G 28/39 GHz dual-band low-IF receiver including the frequency reconfigurable LNA, where 28 and 39 GHz bands are set as the desired and image frequency pairs. To achieve better noise performance, a wideband gain stage is used to cover both bands, and a frequency reconfigurable block is utilized to split the signals into 28 GHz low-band (LB) and 39 GHz high-band (HB). In this way, for each target operating band, more design and optimization flexibilities are gained in the output stage design, thereby improving the amplifier gain, noise figure and out-of-band signal rejection performance. In addition, to minimize the chip area and further improve the out-of-band signal rejection, a low-loss and area-efficient impedance matching network is proposed by utilizing the magnetic-capacitive coupling transformer.

II. Circuit Design

A. Frequency Reconfigurable LNA

Fig. 2 shows the proposed LNA schematic, which consists of an input CS gain stage, two parallel frequency reconfigurable CG gain stages, and output cascode stages. The input CS stage

This work was supported in part by the National Key Research and Development Program, China, under Subject (No.2023YFB4403803), and in part by the Major Key Project of Peng Cheng Laboratory (PCL). (*Corresponding authors: Lianming Li, Xujun Ma.*)

Depeng Cheng is with Purple Mountain Laboratories, Nanjing 211100, China.

Xujun Ma is with Télécom SudParis, Institut Polytechnique de Paris, 91120 Palaiseau, France.

Xin Chen, Qin Chen, and Lianming Li are with the National Mobile Communication Research Laboratory, Southeast University, Nanjing 211189, China., also with Purple Mountain Laboratories, Nanjing 211100, China. (e-mail: lianming.li@seu.edu.cn)

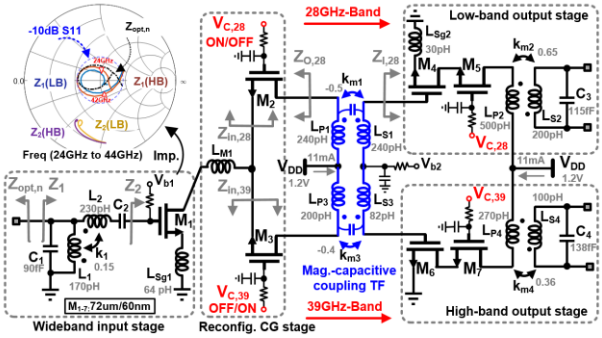

Fig. 2. The proposed frequency reconfigurable LNA schematic, and simulated Z_1, Z_2, and optimal impedance ($Z_{opt,n}$) for noise matching in Smith chart.

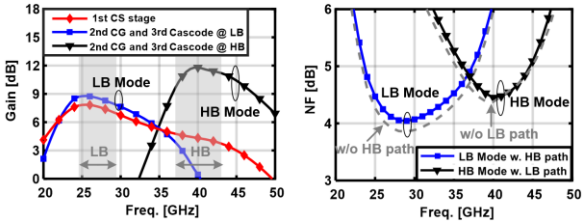

(a) (b)

Fig. 3. (a) Simulated gains of the input CS and CG stages together with the 3rd cascode stage, and (b) NF with/without the disabled CG signal path loading effect in the LB/HB modes.

is realized with the inductive source degeneration technique and an input compact ladder-based transformer network. Benefitting from the transformer network multi-resonance feature, both broadband impedance and noise matching are realized, as illustrated in Fig. 2.

With two parallel transistors, $M_{2,3}$, the frequency reconfigurable CG gain stages are realized. Controlled by two digital bits, $V_{C,28}$/$V_{C,39}$, one CG gain stage is disabled and the broadband input RF signal could be split into the 24.25-29.5 GHz LB or 37-43.5 GHz HB signal path, thereby realizing the band-switching frequency reconfigurable functionality and reducing the loading effects of inactive signal path. For 28 and 39 GHz operating bands, the magnetic-capacitive coupling transformer-based impedance matching network is introduced in the following two cascode gain stages. For performance illustration, Fig.3 (a) shows simulated gains of the input CS and CG stages together with the output cascode stages in 28 and 39 GHz bands, respectively. As indicated, the first gain stage exhibits wideband characteristics, while the last two stages have very good power gain and significantly improve the out-of-band signal rejection performance due to the relatively narrow operating bandwidth benefits of the proposed band-switching solution. It is worth noting, different from the HB output stage, the LB cascode gain stage utilizes the inductive source degeneration technique to balance its gain and linearity performance. For better illustration of the disabled signal path loading effect, Fig.3 (b) shows the simulated NF performance. As indicated, for the cases with and without the disabled CG gain stage, the amplifier NF has very small difference, proving that the proposed band-switching frequency reconfigurable solution has less effect on the amplifier noise performance.

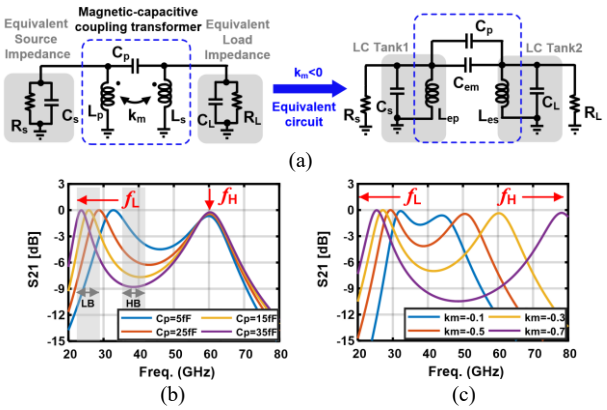

(a) (b) (c)

Fig. 4. (a) The equivalent circuit of low-band inter-stage magnetic-capacitive coupling transformer-based matching network, and (b) simulated frequency response with different C_p values and k_m=-0.5, and (c) with different k_m values, C_p=20fF, R_s=238Ω, C_s=50fF, R_L=294Ω, C_L=65fF, and L_p=L_s=240pH.

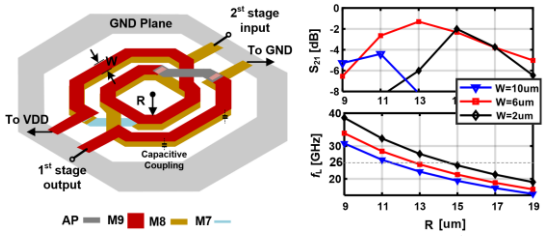

(a) (b)

Fig. 5. Low-band inter-stage matching network (a) layout, and (b) effects of transformer physical parameters, i.e. the width (W) and radius (R), on f_L and insertion loss at 26 GHz.

B. Magnetic-Capacitive Coupling Transformer-Based In-band Matching and Out-of-band Signal Rejection Technique

In this design, to further achieve low in-band insertion loss and high out-of-band signal rejection with a compact chip size, a magnetic-capacitive coupling transformer-based impedance matching technique is introduced in the 28/39 GHz signal paths. To illustrate its working principle, the equivalent circuit of the LB inter-stage matching network is used, as shown in Fig. 4(a). As indicated, with the source and load equivalent circuits, the matching network is equivalent to a capacitive-coupled resonator and the capacitive and magnetic coupling signals will add up positively due to a negative magnetic coupling coefficient k_m. To gain more design insight, two transmission poles, f_H and f_L are derived as follows, in which C_s=C_L=C and L_{ep}=L_{es}=L_e are assumed while R_S and R_L loading effects are neglected for calculation and analysis convenience.

$$f_H = \frac{1}{2\pi\sqrt{L_e C}},\ f_L = \frac{1}{2\pi\sqrt{L_e(2C_{em}+2C_p+C)}} \quad (1)$$

where the magnetic coupling equivalent inductor L_e and capacitor C_{em} could be estimated as below

$$L_e = L_p L_s \frac{1-k_m^2}{L_s - k_m\sqrt{L_p L_s}},\ C_{em} = \frac{k_m}{\omega^2\sqrt{L_p L_s}(1-k_m^2)} \quad (2)$$

Considering above mentioned requirements of low in-band insertion loss and high out-of-band signal rejection, f_L is positioned for the in-band signal, while f_H is set for the out-of-band signal spectral shaping. In particular, considering the LB second-stage output impedance, $Z_{O,28}$, and the third-stage input impedance, $Z_{I,28}$, the effects of C_p and k_m on

TABLE I. COMPARISON WITH STATE-OF-THE-ART MULTI-BAND LNAS

	[8] MWCL'22	[9] TCAS II'21	[11] TCAS I'18		[10] TMTT' 23		[12] MWCL'22		[14] MWCL'22		**This Work**	
Design	Wideband	Wideband	Concurrent		Concurrent		Band Switching		Band Switching		**Band Switching**	
Freq. (GHz)	18-44	21-41	21.5	36	28	39	26-30	37-40	28.5	38	**28**	**39**
3-dB BW	26	20	7.5	12.6	6.6	4.7	6*	4*	5.3	9.4	**7.5**	**7.5**
Peak Gain (dB)	19.5	28.5	16.6	16.7	22	16	13.68	13.04	11.1	8.5	**16.6**	**15**
IIP3 (dBm)	N/A	-10.8#	-14.9	-16.8	-17*	-10.3	-7.15	-6.85	-0.9#	3#	**-2.5**	**-6.6**
IP_{1dB} (dBm)	-18.5	-20.4	-24.3	-26.9	-26*	-17.2	-15.2	-16	-10.5	-6.6	**-12.1**	**-16.5**
NF (dB)	2.6-3.5	2.7	4.2	4.3	2.55	4.75	3.84	4.47	3.49	4.01	**4.06**	**4.46**
P_{dc}(mW)	27.6	32	73.8		18		11.6		16.8		**26.4**	
Core Area (mm^2)	0.16	0.28*	0.69		0.59*		0.17		0.12		**0.1**	
FoM_1**/FoM_2***	1.275/7.96	1.4/5*	N/A		N/A		1.3/7.64	0.83/4.88	1.57*/13.08*	1.95*/16.25*	**2.56/25.6**	**1.21/12.1**
Process.	65-nm CMOS	65-nm CMOS	180-nm SiGe		22-nm FDSOI		65-nm CMOS		65-nm CMOS		**65-nm CMOS**	

*Deduced from the table and figure. #Estimated using IP_{1dB}+9.6 dB.

** $FoM_1 = [G \times IIP3(mW) \times BW(GHz)] / [(F-1) \times P_{DC}(mW)]$. *** $FoM_2 = [G \times IIP3(mW) \times BW(GHz)] / [(F-1) \times P_{DC}(mW) \times Core\ Size(mm^2)]$.

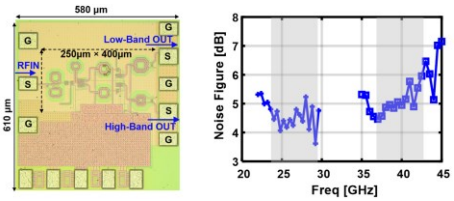

(a) (b)

Fig.6 (a) Die micrograph, and (b) measured LNA NF.

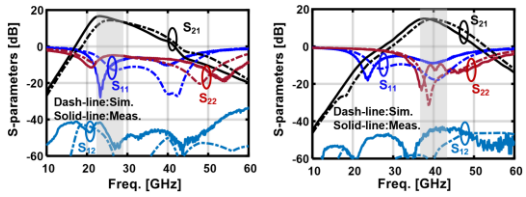

(a) (b)

Fig. 7 Simulated and measured LNA S-parameters in (a) LB, and (b) HB modes.

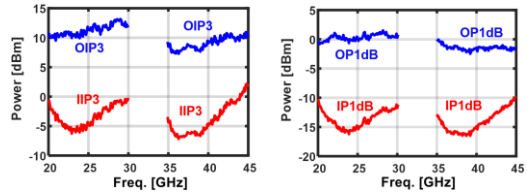

(a) (b)

Fig.8 Measured (a) IIP3 and OIP3, and (b) IP_{1dB} and OP_{1dB} of the LNA.

the impedance matching network are evaluated. As depicted in Fig. 4(b) and equation (1), f_H is independent of C_p, while f_L is mainly determined by C_p+C_{em}. Thus, C_p can be tuned for the in-band matching without affecting the out-of-band frequency response characteristic. As indicated in Fig. 4(c), k_m affects f_H and f_L spacing, and a high k_m is preferred for high out-of-band signal rejection performance.

Based on above calculation and simulation results, dedicated efforts are devoted to the optimization of the inductor magnetic and capacitive coupling, and LB and HB inter-stage matching network are well designed. As shown in Fig. 5(a), the proposed magnetic-capacitive coupling transformer is realized with a stacked coupled transformer. In this way, C_p is realized with the parasitic capacitor of the transformer two adjacent metal layers, and a desired high coupling factor k_m is achieved simultaneously. The transformer layout and performance optimization are undertaken with its two main design parameters, i.e. the width (W) and radius (R). As shown in Fig .5(b), with optimized W and R of 6 and 13 um, respectively, 26 GHz f_L and 1.6-dB insertion loss are achieved with only 62×64 um^2 chip area.

III. MEASUREMENT RESULTS

As depicted in Fig. 6(a), fabricated in a 65-nm CMOS process, the proposed LNA occupies 610 × 580 μm^2 with a core area of only 0.1 mm^2, and it consumes 26.4 mW from a 1.2 V supply voltage. The performance of the LNA chip is measured on wafer with the inactive signal path terminated with a 50-Ω load. As indicated in Fig. 6(b), the measured NF ranges from 4.06 to 5.2 dB and from 4.46 to 6.5 dB in the 28 GHz LB and 39 GHz HB, respectively. Fig. 7(a) and (b) compare the simulated and measured S-parameters. Clearly, at 28/39 GHz bands, the LNA demonstrates a maximum gain of 16.6 /15 dB, a 3-dB bandwidth of 7.5/7.5GHz, and an excellent wideband S_{11}. Moreover, the measured S-parameters exhibit more than 8/10.5 dB out-of-band rejection. It should be noticed that the measurement and simulation results agree well with each other, and the mismatch is proved to be mainly caused by the underestimated parasitic inductance of the power supply. Moreover, as shown in Fig. 8 (a) and (b), the LNA demonstrates an IP_{1dB} and IIP3 of above -16.5 and -7 dBm, respectively.

Table I compares the performance of the proposed LNA with the state-of-the-art 5G dual-band mm-wave amplifiers. Compared with other wideband/concurrent/band-switching LNAs, the proposed LNA exhibits a competitive overall performance with the most compact chip area. And a relatively large dc power is consumed for high linearity performance.

IV. CONCLUSIONS

This letter presents a frequency reconfigurable LNA in a 65-nm CMOS process for 5G 28/39 GHz bands applications. Leveraging an active CG band-switching solution, more design and optimization flexibilities are gained, thereby improving the LNA gain, noise figure and out-of-band signal rejection performance. Moreover, with theoretical analysis and simulations, the operation mechanism and design insight of the magnetic-capacitive coupling transformer impedance matching are illustrated, and the LNA achieves competitive overall performance with a power gain of 16.6/15 dB, a minimum NF of 4.06/4.46 dB at 28/39GHz bands, making it attractive for future 5G mm-wave multi-band receivers.

REFERENCES

[1] R. Garg et al., “A 28 GHz/39 GHz Dual-Band Four-Element MIMO RX with Beamspace Multiplexing at IF in 65-nm CMOS,” *2022 IEEE Radio Frequency Integrated Circuits Symposium (RFIC)*, Denver, CO, USA, 2022, pp. 7-10.

[2] S. Wang and G. M. Rebeiz, “Dual-Band 28- and 39-GHz Phased Arrays for Multistandard 5G Applications,” *IEEE Transactions on Microwave Theory and Techniques*, vol. 71, no. 1, pp. 339-349, Jan. 2023.

[3] J. Lee, H. Jin, G. Lee, E. -T. Sung and S. Hong, “A 28/37 GHz Frequency Reconfigurable Dual-Band Beamforming Front-End IC for 5G NR,” 2023 *IEEE Radio Frequency Integrated Circuits Symposium (RFIC)*, San Diego, CA, USA, 2023, pp. 45-48.

[4] Y. Zhang et al., “A Power-Efficient CMOS Multi-Band Phased-Array Receiver Covering 24–71-GHz Utilizing Harmonic-Selection Technique With 36-dB Inter-Band Blocker Tolerance for 5G NR,” *IEEE Journal of Solid-State Circuits*, vol. 57, no. 12, pp. 3617-3630, Dec. 2022.

[5] C. Zhao et al., “A K-/Ka-Band Broadband Low-Noise Amplifier Based on the Multiple Resonant Frequency Technique,” *IEEE Transactions on Circuits and Systems I: Regular Papers*, vol. 69, no. 8, pp. 3202-3211, Aug. 2022.

[6] O. Kazan, Z. Hu, L. Li, A. Alhamed and G. M. Rebeiz, "An 8-Channel 5–33-GHz Transmit Phased Array Beamforming IC with 10.8–14.7-dBm Psat for C-, X-, Ku-, and Ka-Band SATCOM," in IEEE Transactions on Microwave Theory and Techniques, vol. 71, no. 5, pp. 2029-2039, May 2023.

[7] H. Chen, H. Zhu, L. Wu, W. Che and Q. Xue, "A Wideband CMOS LNA Using Transformer-Based Input Matching and Pole-Tuning Technique," in IEEE Transactions on Microwave Theory and Techniques, vol. 69, no. 7, pp. 3335-3347, July 2021.

[8] R. Wang, C. Li, J. Zhang, S. Yin, W. Zhu and Y. Wang, “A 18–44 GHz Low Noise Amplifier with Input Matching and Bandwidth Extension Techniques,” *IEEE Microwave and Wireless Components Letters*, vol. 32, no. 9, pp. 1083-1086, Sept. 2022.

[9] Y. Yu et al., “A 21-to-41-GHz High-Gain Low Noise Amplifier with Triple-Coupled Technique for Multiband Wireless Applications,” *IEEE Transactions on Circuits and Systems II: Express Briefs*, vol. 68, no. 6, pp. 1857-1861, June 2021.

[10] J. Fu, M. G. Bardeh, J. Paramesh and K. Entesari, “A Millimeter-Wave Concurrent LNA in 22-nm CMOS FDSOI for 5G Applications,” *IEEE Transactions on Microwave Theory and Techniques*, vol. 71, no. 3, pp. 1031-1043, March 2023.

[11] J. Lee and C. Nguyen, “A K-/Ka -Band Concurrent Dual-Band Single-Ended Input to Differential Output Low-Noise Amplifier Employing a Novel Transformer Feedback Dual-Band Load,” *IEEE Transactions on Circuits and Systems I: Regular Papers*, vol. 65, no. 9, pp. 2679-2690, Sept. 2018.

[12] B. Bae, E. Kim, S. Kim and J. Han, “Dual-Band CMOS Low-Noise Amplifier Employing Transformer-Based Band-Switchable Load for 5G NR FR2 Applications,” *IEEE Microwave and Wireless Technology Letters*, vol. 33, no. 3, pp. 319-322, March 2023.

[13] Z. Wang et al., “A Ka-Band Switchable LNA with 2.4-dB NF Employing a Varactor-Based Tunable Network,” IEEE Microwave and Wireless Components Letters, vol. 31, no. 4, pp. 385-388, April 2021.

[14] S. Lee and S. Hong, “Frequency-Reconfigurable Dual-Band Low-Noise Amplifier with Interstage Gm-Boosting for Millimeter-Wave 5G Communication,” *IEEE Microwave and Wireless Technology Letters*, vol. 33, no. 4, pp. 463-466, April 2023.